# Cloud Detection in SEVIRI Images by Non-Homogeneous Temporal Markov Random Fields

Paolo Addesso, Roberto Conte, Maurizio Longo, Rocco Restaino and Gemine Vivone
*University of Salerno, D.I.I.I.E, Fisciano, Italy;*
*{paddesso,rconte,longo,restaino,gvivone}@unisa.it*

**Abstract.** Cloud detection is a preliminary step in most earth observation procedures employing remotely sensed data. Fire, sea and urban areas satellite monitoring, for instance, can be strongly impaired if the effects of clouds are not properly taken into account, e.g. by constructing an accurate cloud mask. In this paper we exploit the Markov Random Field (MRF) to draw a computationally light cloud detection algorithm. MRF is a consolidated statistical methodology to model spatial correlation among neighboring pixels in an image. Some extensions such as Extended Markov Random Fields (EMRF) take into account temporal correlation between subsequent images, by means of an homogeneous energy term in the Gibbs distribution along the estimated motion direction. Here we introduce a novel approach, in which the prior energy includes a non-homogeneous term depending on the relative position, specifically the connection level, of the cloud pixels detected in the previous image. In this way, we better match the cloud dynamics, in terms of both position and shape. A comparative performance evaluation on simulated cloudy images is carried on, showing that the said method outperforms standard MRF and EMRF based algorithms. A first analysis on real images of Sardinia island from SEVIRI sensor is in keeping with the above result.

**Keywords.** Cloud Detection, Cloud tracking, Maximum A posteriori Probability (MAP), Markov Random Field (MRF), SEVIRI

## 1. Introduction

Cloud detection is a very important issue in extracting information of geophysical, geomorphologic and meteorological interest from remotely sensed images.

According to the particular application, clouds act for an unsolicited corruption of the available data or, rather, as a source of information to infer relevant properties of the atmosphere [2]. Sea and urban areas satellite monitoring, for instance, is strongly impaired if the presence of clouds is not properly taken into account. Algorithms for fire detection experience a double negative effect from the presence of cloudy pixels: the latter can be easily misclassified as fire pixels due to the increased brightness temperature, as well as clouds can hide an effectively burning zone [3]. Precise sea surface temperature estimates can be achieved by sensors operating at Thermal InfraRed (TIR) frequencies only after assuring a proper preliminary cloud screening phase [4]. Oppositely, accurate evaluation of positions and movements of the clouds masses is the basis for climate and meteorological applications, ranging from wind fields and hurricane tracking to data assimilation and numerical weather prediction [5]. Therefore the production of a cloud mask represents a needed preliminary step for their correct working [2].

The cloudy/non-cloudy classification of pixels can be performed by several approaches. Due to their simplicity, pixel-wise approaches have been largely explored in the past by means of both supervised and unsupervised techniques. The former relies on a preliminary feature space selection performed by an expert. The subsequent class association step can be carried out, through Discriminant Analysis (DA) as in [6], Probabilistic Neural Networks (PNN) [8], or Support Vector Machines (SVM) [9]. Unsupervised procedures, either parametric, based on the estimation of the cha-

racterizing distribution quantities [11] or non-parametric [2] have been used. Since unsupervised classification cannot take advantage of a guided setup, it's prone to produce inaccurate results. On the other side, supervised approaches can suffer from inadequacy of the training set as shown in [10].

A significant progress in the design of a cloud classification algorithm, can be obtained by taking into account the correlation of the label of a generic pixel with those of its neighbors. Among these approaches, one of the most powerful relies on the application of the Markov Random Fields (MRF) theory that provides a convenient and consistent way of modeling context-dependent entities, such as image pixels values [1]. For these reasons and, crucially, for computational affordability, MRFs have been widely employed to solve vision problems at all levels.

While pixels inside the cloud body are typically well classified, those close to the border are often misclassified due to lower contrast of cloud edges against the land or sea background [12]. However, an additional discriminating feature of a cloud edge respect to the static background consists possibly in its motion. This concept calls for exploiting temporal information in addition to purely spatial information as in classical approaches [13], [14].

In [15] we introduce an a-priori term stemming for the predicted cloud pixel positions and show performance improvements with respect to classical spatial MRF and spatio/temporal EMRF (Extended MRF) [18], Bayesian classification. This prior term is computed by approximating cloud volumes by circumscribing rectangles.

This simple approach turns out to lack in describing extended and rugged clouds, eventually resulting in misclassification rate worsen. In this paper we present a level of connection based a-priori to overcome this problem and we show, in Section 3, how this new technique improves the performances obtained in [15]. To this aim we employed a simple cloud simulator to get a set of ground truths for heterogeneous situations. Finally, results in keeping with simulated test are provided for real SEVIRI images.

## 2. Methods

In this section, cloud classification using *Maximum A posteriori Probability-Markov Random Field* (MAP-MRF) framework is presented [1].

This probabilistic approach is based on the hypothesis that the labels of each pixel (also named site) $i \in S$ of an image (where $S$ is the pixel index set), assuming values in $L = \{0,1\} = \{$*non-cloud*, *cloud*$\}$, constitutes a MRF $F$.

The estimate $\hat{f}$ of the actual label realization $F = f$ is achieved by means of the MAP rule,

$$\hat{f} = \underset{f}{\operatorname{argmax}} [\, \mathrm{p}(f|\, d)\,] = \underset{\mathrm{f}}{\operatorname{argmax}} [\, \mathrm{p}(d|f) \cdot \mathrm{p}(f)\,]$$

where $p(d \mid f)$ is the data *likelihood* and $p(f)$ is the *a priori probability* of the classified image.

One of the main theoretical results in MRF theory is the equivalence with a *Gibbs Random Field* (GRF) (or Hammersley-Clifford theorem) [1], that let us to express the joint probability of a MRF as:

$$p_T(f) \propto \exp[\, -\frac{1}{T} U(f)\,] \tag{1}$$

where $T$ is a constant called the *temperature*, which shall be assumed to be 1 unless otherwise stated, and $U(f)$ is the *energy function*.

A common choice is a likelihood of the kind

$$p(d \mid f) \propto \exp[-U(d \mid f)]$$

that allows to write, together with (1), the posterior probability as

$$p(f \mid d) \propto \exp[-U(d \mid f)]\exp[-U(f)] \propto \exp[-U(f \mid d)].$$

Applying the MAP estimator to the posterior probability, we have:

$$\hat{f} = \arg\min_{f}[U(f \mid d)] = \arg\min_{f}[U(d \mid f) + U(f)].$$

In general, the minimization of a non-convex function has no closed solution. Thanks to the Markov property, that limit the interaction between neighbor labels up to a limited area surrounding each pixel, this task can be afforded by very efficient algorithms, such as the Simulated Annealing [1].

The most used neighboring model relies upon the (2DI) *Ising model* that contains terms describing interactions among up to two sites. For this model, $U(f)$ can be written as

$$U(f) = \sum_{i \in S} \sum_{j \in N_i} \beta_s \cdot \delta(f_i - f_j) \tag{2}$$

where $f_i$ and $f_j$ are the labels of pixel $i$ and $j$ respectively, $N_i$ is the spatial neighborhood of the pixel $i$ that, in the Ising model adopted here, includes only vertical and horizontal pixels respect to the site $i$ and $\beta_s$ is defined as the *spatial* interaction *coefficient*.

For the data likelihood, we assume a factorized Laplace distribution although other factorized distributions are allowed:

$$U(d_i \mid f_i) = \begin{cases} |d_i - \mu_1|, & \text{if } f_i = 1, \\ |d_i - \mu_0|, & \text{if } f_i = 0, \end{cases}$$

where $\mu_1$ and $\mu_0$ are the (estimated) centroids of the two classes and the factorized form is allowed by the conditional independence hypothesis of the pixel values given the assigned label.

The aim of the paper is to investigate the possibility of improving the spatio-temporal approach proposed in [15] where a generalization of the Ising model (2) is presented to take into account the temporal dependencies among pixels. We propose here a different way to include the a-priori information deriving from the cloud motion tracking.

In the cited approach, since the cloudy pixels compose blob-like regions, we compute, in a given image at time *k - 1*, the rectangular boxes (or *bounding boxes*) containing all the 8-connected pixels labeled as cloud and track their evolution. In particular, after estimating the cross covariance coefficients [17] between image at time *k - 1* and that at time *k*, we are able to associate at each bounding box (and consequently at each pixel therein contained) a motion vector, as shown in Fig.1. This allows to define, for each pixel, its ***time-neighborhood***. So in the following we propose to use different algorithms:

- the *3D-Ising-like* algorithm (3DI) already presented in [18];
- the *3D-Penalized* algorithm (3DP) [15].

These algorithms consist in simply generalizing the energy function (2) by adding a time neighbor dependent term. In order to compute them, the first step consists in calculating a prediction of the cloud positions at the frame *k + 1*, given the classification at the frame *k*. This is a classical multi-target tracking problem. We use a MCC method based on the *Normalized Cross Covariance Coefficient* (NCCCoef) [17].

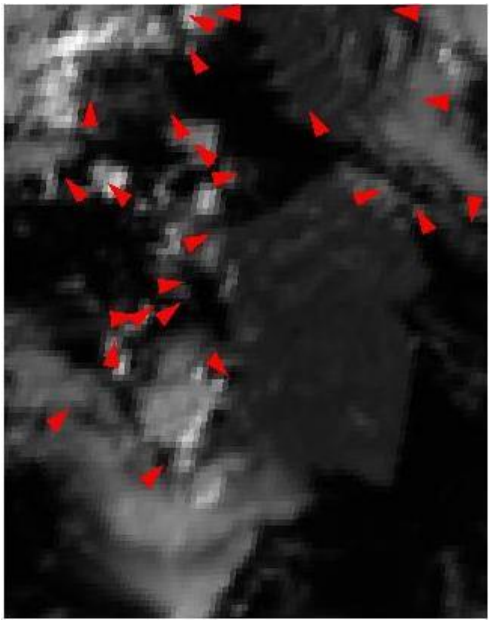

Figure 1: An example of cloud motion estimation with the algorithm proposed in this section. Red arrows represent directions of motion of the cloud objects.

### *3.1 3D-Penalized algorithm (3DP)*

The approach proposed in [15], called 3DP (3D-Penalized), relies in defining the first order potential $V_1(\mathrm{f_i})$ as:

$$V_1(f_i) = \begin{cases} \beta_t \cdot [1 - \lambda(i)], & \text{if } f_i = 1, \\ \beta_t \cdot \lambda(i), & \text{if } f_i = 0, \end{cases}$$

where $\beta_t$ is called *temporal interaction coefficient* and $\lambda(i)$ is the *penalty function*. The latter was defined as unitary at the center of the bounding boxes representing the predicted clouds' positions and as linearly decreasing with the distance from center. An instance of such density function is shown in Fig. 2.

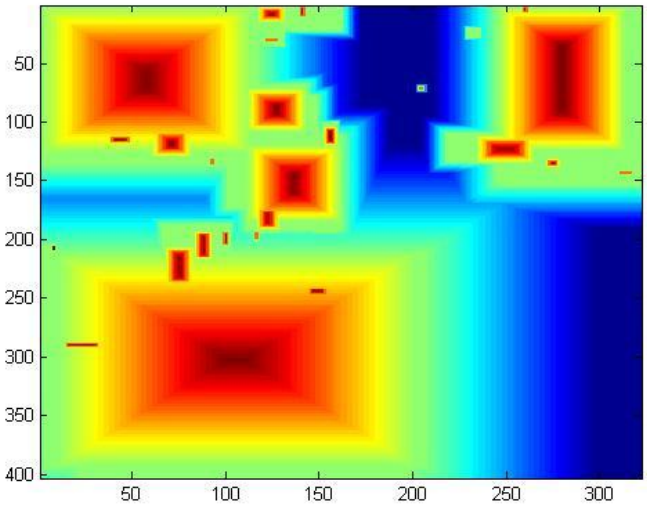


Figure 2: An example of penalty term based on bounding boxes.

In the presence of big and merging clouds a detailed expression for the function $\lambda$ can be more useful. For that reason, we define a pixel to be *"8-connected"* if it is labeled as cloud, as well as all the pixels belonging to its *8*-neighborhood. The latter is composed by the adjacent pixels in vertical, horizontal and diagonal directions. Moreover a pixel is said to be *"N-times 8-connected"* if it is *8-connected* and all its neighbors are *"(N-1)-times 8-connected"*. The *"level of connection* $L_i$*"* is defined as the maximum *N* such that pixel *i* is *"N times 8-connected"*. Mathematically, we have:

$$L_i = \max_N \{ i \text{ is } N\text{-times } 8\text{-connected} \}.$$

Furthermore, if $C = \{C_j\}_{j=1}^{Nc}$ is the collection of the $N_c$ disjoint detected clouds, we define the quantities

$$M(C_j) = \max_{i \in C_j} L_i$$

and the metric

$$d(i, C) = \min_{C_j \in C} d(i, C_j).$$

Finally, the proposed density function is described by the expressions:

$$\lambda_i = \begin{cases} \lambda_E + (1 - \lambda_E) \dfrac{L_i}{M(C_j)}, & \text{if } i \in C_j, \\ \lambda_E, & \text{if } d(i, C) < \Delta, \\ \lambda_E \cdot \exp\{-\alpha \cdot | d(i, C) - \Delta |\}, & \text{otherwise.} \end{cases} \tag{3}$$

In this expression $\Delta$ is a coefficient that allows to expand the cloud range, $\alpha$ is a decay exponent and $\lambda_E$ is the density of a cloud pixel on the cloud edges. An instance of such density function is shown in Fig. 3.

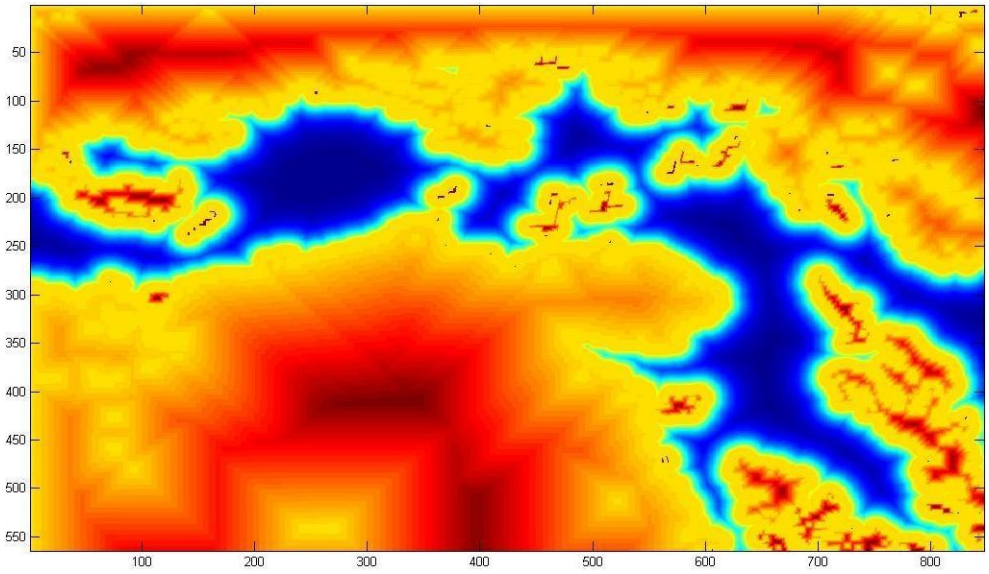


Figure 3: An example of penalty term as in (3).

## 3. Results

In this section, a performance comparison of the algorithms presented above (resumed in **Table 1**) is carried out under various instances. Firstly, we report the results relative to data simulated by means of a simple cloud behavior emulator. This step was performed in order to obtain a reliable ground truth. Subsequently we show the results achieved on SEVIRI images, classified by *"naked-eye"*.

**Table 1.** Glossary

| Abbreviation | Name |
|---|---|
| 3DI | *3D-Ising-like* (also named *Extended Markov Random Field* in [18]) |
| 2DI | *2D Ising* |
| 3DP-BB | *3D-Penalized* – bounding box |
| 3DP-LC | *3D-Penalized* – levels of connection |

### *4.1 Simulated analysis*

In order to carry out a preliminary analysis of the results obtained by the presented algorithms with several environment conditions, we developed a simulator of cloud-like blobs that is able to account for a small set of cloud peculiar features, as for example motion, deformation, etc. In particular, the simulator produces an image sequence in which the birth, evolution and death process of a set of blobs is superimposed to a remotely sensed image. During their lifetime the cloud-like shapes are rotated, translated, dilated and eroded by means of geometrical and morphological operators. Final-

ly, in order to achieve more realistic error estimation, the images resulting from geometric manipulations were degraded with additive Gaussian noise and salt and pepper noise.
A set of 21 tests have been performed. In Fig. 4 the detailed results for each test case are presented in terms of the average misclassification rate, while in Table **2** the average results are shown.

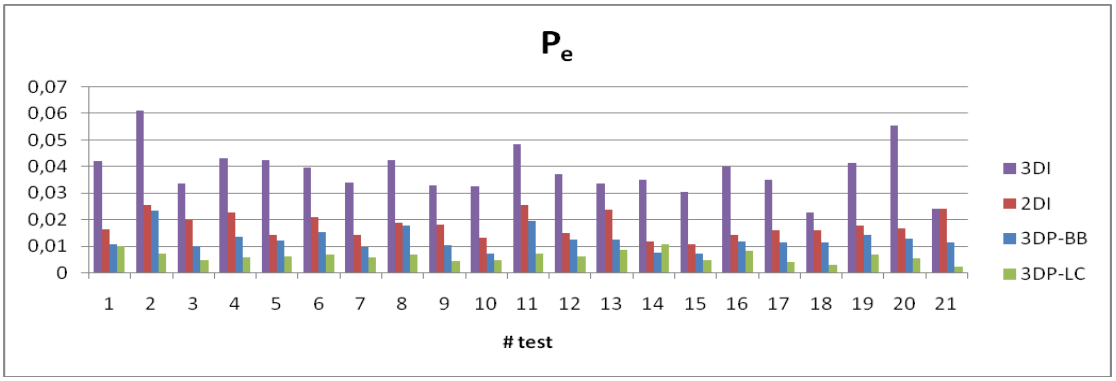


Figure 4: Detailed misclassification rate of the 4 algorithms in the 21 test cases.

**Table 2.** Misclassification rate of the 4 algorithms averaged on the whole test set..

| | $P_e$ |
|---|---|
| 3DI | 0.038 |
| 2DI | 0.018 |
| 3DP-BB | 0.012 |
| 3DP-LC | 0.006 |

In Fig. 4, we can see that the 3DI algorithm achieves performances comparable to the 2DI algorithm only when the effects of cloud deformations are less important than translations (test #21). The 3DP-BB algorithm, on the other hand, always yields better performance compared in respect to the 3DI and 2DI algorithms. The advantage is more evident when morphological operators affect seriously the cloud shape (test #14, #15 and #20) and the number of clouds is very high (test #17). In contrast, poorer performances are achieved with very high noise (test #2), significant rotations (test #5) and high cloud birth rate (test #8).

On the other hand, the 3DP-LC always obtains the overall best performances exclusive of test case #14 where high deformations renders the cloud pixels' estimation hardly predictable by a linear translation. On the contrary, best results are obtained in the test #21 thanks to the absence of deformations. In summary, the map proposed in this contribution gives poor results when there are big errors in the motion estimation phase and/or very high deformations in targets are present.

In any case, simulations confirm that one of the main objectives of the method, i.e., the limited increase of computational effort, is attained by both 3DP algorithms, being the processing time not longer than 1.25 times that of 2DI. However, it's worthy to note that 3DP-BB algorithm processing time doesn't depend on cloud dimensions, while 3DP-LC computation times increases with the cloud extension.

### *4.2 Real SEVIRI images results*

Real data tests have been performed on images acquired by the SEVIRI sensor, in the band VIS 0.8. In this case, no effective ground truth is available for comparing the cloud classification algorithm

performances. To furnish a quantitative measure of the performances, we used a simple MATLAB routine to select by ”naked-eye” the cloud regions and achieve the needed ground truth on real data images of Sardinia island.

In Fig. 5, we can see that the minimum tof the error probability versus the $\beta_t$ parameter is found slightly below $\mu_1 - \mu_0$ (about 100). Moreover, we can note that in this area the algorithm with the new connection based map (3DP-LC) achieve better results, as expected from the simulative setup.

In Figs. 6-8 we report a robustness analysis of the 3DP-LC algorithm that has been performed by evaluating misclassification rate in function of each single parameter of the LC-map. Noticeable variations of the misclassification rate are observed only with the parameter $\lambda_E$ , that entails significant increase of the false alarms when its value is greater than 0.65.

Figs. 9 and 10, permit to compare the classification obtained with the four algorithms presented. In particular, in Fig. 9, the 3DP-BB algorithm is put side by side with the algorithms present in the literature, while, in Fig. 10, we compare the 3DP methods differing for the penalty map to underline differences in the classification phase. We report there the label differences of the cited algorithms, defined as pixel detected by the first algorithm and not by the second. Visual analysis of Fig. 9 underlines the significant enhancement of the detection capabilities of the proposed algorithm. Furthermore Fig. 10 shows that the improvements achieved by exploiting the level of connection map is mainly due to the increased accuracy on the ruggest parts of the cloud masses.

With regard to the computation load comparison between the 3DP-BB and the 3DP-LC algorithms, it is useful to report how the difference is very limited in this case because no wide clouds are in the scene.

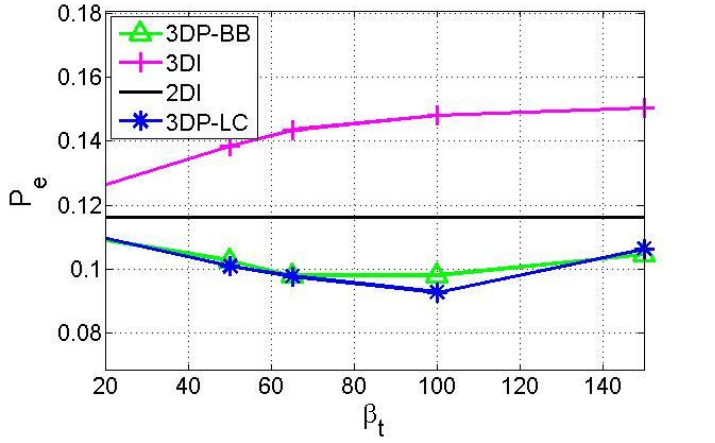


Figure 5: Misclassification rate plotted against the $\beta_t$ parameter.

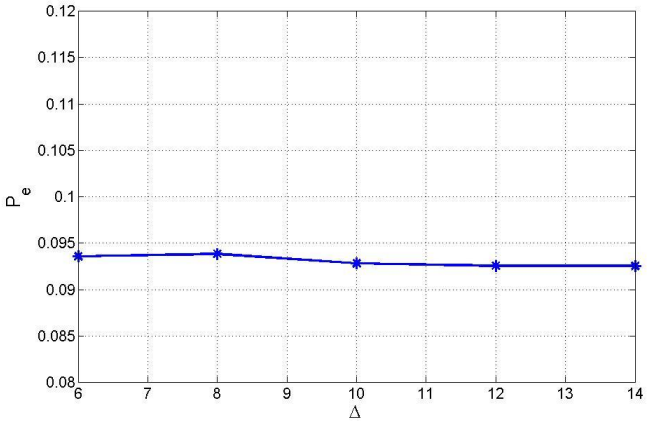


Figure 6: Misclassification rate as a function of the Δ parameter.

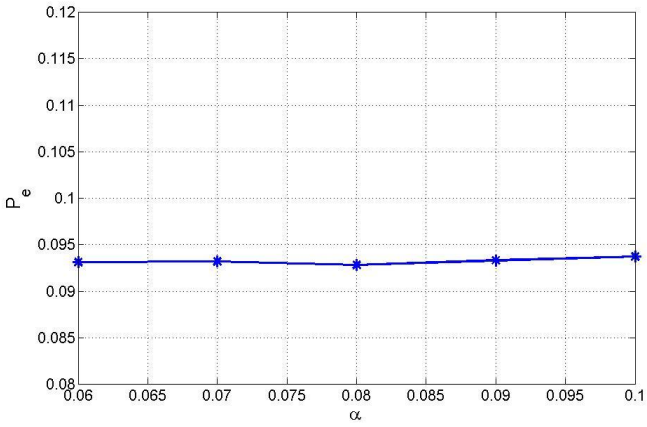


Figure 7: Misclassification rate as a function of the α parameter..

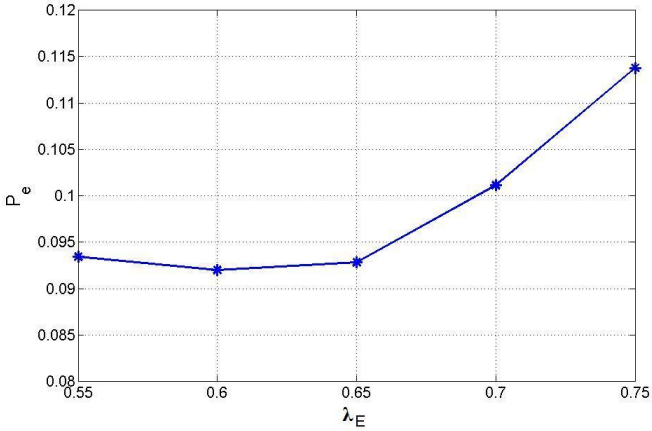


Figure 8: Misclassification rate as a function of the $\lambda_E$ parameter.

..

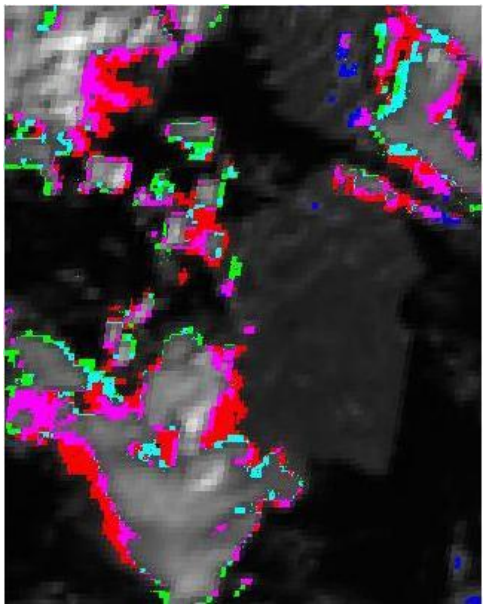

Figure 9: Classification differences among the 3DP-BB, 2DI and 3DI algorithms: in magenta the label differences betweeny 3DP-BB and 3DI, in cyan the differences between 3DP-BB and 2DI, in red the differences between 3DP-BB and both 2DI and 3DI, in blue the differences between 2DI and 3DP-BB and in green the differences between 3DI and 3DP-BB.

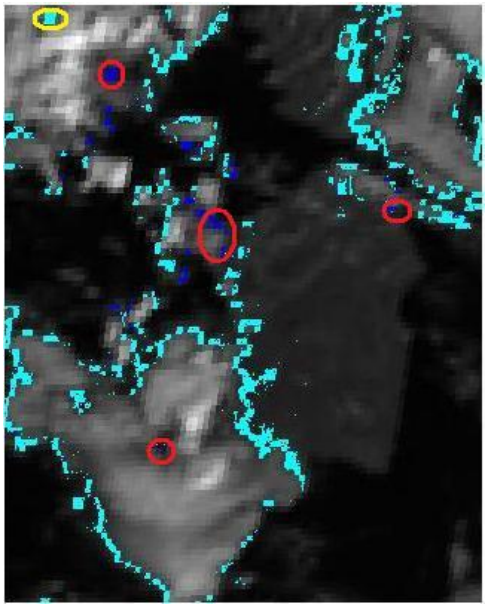

Figure 10: Classification differences between the 3DP-BB and 3DP-LC algorithms: in cyan the difference between 3DP-LC and 3DP-BB and in blue the difference between 3DP-LC and 3DP-BB. Moreover, the false alarms of the 3DP-BB and 3DP-LC algorithms have been highlighted with red and yellow circles respectively.

## 4. Conclusions

In this paper we study a cloud detection algorithm based on the MAP-MRF framework. With the aim of improving the performances of the Bayesian estimator we use an approach that takes into

account the cloud positions in the previous image, as well as their motion between images. The Gibbs distribution form of the posterior density is preserved through a simple modification of the corresponding energy. We introduced a penalty term that strongly depends on the cloud masses shape, thus permitting to fully exploit the possibilities offered by this spatio-temporal approach.
The method imply an increase of the computational effort respect to the classical spatial MRF methods, but this drawback turns out to be significant only in the presence of huge cloud masses.

## Acknowledgements

The authors would like to thank Dr. P.G. Marchetti and the Service Support and Ground Segment Technology Section at ESA-ESRIN, Frascati (Italy) for many helpful discussions and for providing the SEVIRI data.

## References

[1] Li S., 2009. *Markov Random Field Modeling in Image Analysis*, (3rdEd. Springer).
[2] Gòmez-Chova L., Camps-Valls G., Calpe-Maravilla J., Guanter L. & Moreno, J. *Cloud-screening algorithm for envisat/meris multispectral images*. IEEE Trans. Geosci. Remote Sens. 45(12), 4105–4118 (Dec. 2007)
[3] Cadau E. & Laneve G. *Improved msg-seviri images cloud masking and evaluation of its impact on the fire detection methods*. Proc. of IEEE Geoscience and Remote Sensing Symposium (IGARSS), vol. 2, pp. 1056–1059 (2008)
[4] Merchant C., Harris A.R., Maturi E. & Maccallum S. *Probabilistic physically based cloud screening of satellite infrared imagery for operational sea surface temperature retrieval*. Q. J. R. Meteorol. Soc. 131(611), 2735–2755 (Oct 2005)
[5] Rohn M., Kelly G.A. & Saunders R. *Impact of new cloud motion wind products from meteosat on nwp analyses and forecasts*. Mon. Weather Rev., 129(9), 2392–2403 (Sep 2002)
[6] Amato U., Antoniadis A., Cuomo V., Cutillo L., Franzese M., Murino L. & Serio C. *Statistical cloud detection from seviri multispectral images*. Remote Sens. Environ. 112(3), 750–766 (Mar 2008)
[7] Andrews R. *Early investigations in optical flow from colour images*. Ph.D. thesis, Queensland University (2003)
[8] Lee Y.,Wahba G. & Ackerman, S. *Cloud classification of satellite radiance data by multi category support vector machines*. J. Atmos. Oceanic Technol. 21, 159–169 (Feb 2004).
[9] Tian B., Shaikh M., Azimi-Sadjadi M., Haar T. & Reinke D. *A study of cloud classification with neural networks using spectral and textural features*. IEEE Trans. Neural Netw. 10(1), 138–151 (Jan 1999).
[10] Gòmez-Chova L., Camps-Valls G., Bruzzone L. & Calpe-Maravilla J. *Map kernel methods for semi-supervised cloud classification*. IEEE Trans.Geosci. Remote Sens. 48(1), 207–220 (Jan 2010).
[11] Schowengerdt R. *Remote Sensing: Models and Methods for Image Processing*. 3rd Ed. Elsevier (2007).
[12] Ackerman S., Strabala K., Menzel W., Frey R., Moeller C. & Gumley L. *Discriminating clear sky from clouds with modis.* J. Geophys. Res. 103(D24), 32141–32157 (Dec 1998).
[13] Mukherjee D. & Acton S. *Cloud tracking by scale space classification*. IEEETrans. Geosci. and Remote Sens. 40(2), 405–415 (Feb 2002).
[14] Papin C., Bouthemy P. & Rochard G. *Unsupervised segmentation of low clouds from infrared meteosat images based on a contextual spatio-temporal labeling approach*. IEEETrans. Geosci. Remote Sens. 40(1), 104–114 (Jan 1993).
[15] Addesso, P., Conte, R., Longo,M., Restaino,R. & Vivone,G. *A computationally efficient method for sequential map-mrf cloud detection*, Proc. ICCSA 2011, Part II, LNCS 6783, pp. 354–365 (2011) in print.
[16] Lempitsky V., Kohli P., Rother C. & Sharp, T. *Image segmentation with a bounding box prior*. 12th IEEE International Conference on Computer Vision. pp. 277–284 (2009).
[17] Marcello J., Eugenio F. & Marques, F. *Cloud motion estimation in seviri image sequences*. Proc. of IEEE Geoscience and Remote Sensing Symposium (IGARSS). vol. 3, pp. 642–645 (2009).
[18] Stolkin R., Hodgetts M., Greig A. & Gilby, J. *Extended markov random fields for predictive image segmentation*. WSPC - Proceedings (2006).